BLIND COMPRESSED SENSING WITH SPARSE DICTIONARIES FOR ACCELERATED DYNAMIC MRI

Sajan Goud Lingala[*] *and Mathews Jacob*[†]

[*] Department of Biomedical Engineering, The University of Iowa, IA, USA
[†] Department of Electrical and Computer Engineering, The University of Iowa, IA, USA

ABSTRACT

Several algorithms that model the voxel time series as a sparse linear combination of basis functions in a fixed dictionary were introduced to recover dynamic MRI data from under sampled Fourier measurements. We have recently demonstrated that the joint estimation of dictionary basis and the sparse coefficients from the k-space data results in improved reconstructions. In this paper, we investigate the use of additional priors on the learned basis functions. Specifically, we assume the basis functions to be sparse in pre-specified transform or operator domains. Our experiments show that this constraint enables the suppression of noisy basis functions, thus further improving the quality of the reconstructions. We demonstrate the usefulness of the proposed method through various reconstruction examples.

1. INTRODUCTION

Dynamic MRI is a key component of many clinical exams such as cardiac, perfusion, and functional imaging. The slow nature of the MR image acquisition scheme and the risk of peripheral nerve stimulation often restricts the achievable spatio-temporal resolution and volume coverage in dynamic MRI. Several acceleration schemes that recover dynamic images from undersampled $k-t$ measurements have been proposed to overcome these problems. They include the classical $x-f$ space packing methods (eg:[1]), low rank models (eg:[2, 3]), compressed sensing (CS) schemes (eg:[4, 5]), combined low rank and CS schemes [3, 6], and more recently blind compressed sensing with learned dictionaries [7].

In this paper, we further develop our previous work on blind compressed sensing (BCS) based dynamic MRI [7]. The BCS framework model the Casorati matrix of the spatio-temporal signal as the product of a sparse coefficient matrix and a dictionary of temporal basis functions; the sparse coefficients and the dictionary basis functions are jointly estimated from under sampled k-space data. The Frobenius norm of the dictionary is upper bounded by a constant to avoid scale ambiguity issues. The proposed scheme provided improved reconstructions of myo-cardial perfusion MRI data, compared to existing methods such as low rank and CS methods [7]. To further validate BCS, we compare it with k-t FOCUSS in the context of highly accelerated cine MRI. Note that the Fourier dictionary used in k-t FOCUSS is more or less optimal due to the periodic cardiac motion. We observe that the some of the basis functions learned by the BCS scheme suffered from noise or alias patterns at such high accelerations, resulting in in speckle-like residual alias artifacts in the reconstructed data (see Fig. 3). This example motivates us to go beyond the framework of blind dictionary learning, with the objective of learning dictionaries with more accurate basis functions.

The main focus of this paper is to improve the BCS algorithm by further constraining the dictionary basis functions. Specifically, we model the Casorati matrix as the product of two matrices $\mathbf{U}$ and $\mathbf{V}$, which are sparse in two transform/operator (denoted by $\mathcal{T}_1$ and $\mathcal{T}_2$, respectively) domains. The main difference of this scheme with the BCS setting is the sparsity penalty on the temporal basis functions. Hence, we term the new model as sparse BCS. The new constraint enables us to inject prior information (eg. smoothness of the basis functions) into the reconstruction algorithm by appropriately choosing $\mathcal{T}_2$. We pose the joint recovery of $\mathbf{U}$ and $\mathbf{V}$ as an optimization problem, where the cost function is a linear combination of data consistency and sparsity penalties on $\mathbf{U}$ and $\mathbf{V}$. We use a majorize minimize alternating minimization strategy to solve the optimization problem. The optimization problem is non-convex; it is convex with respect to one variable, if the other is assumed to be fixed. To minimize the risk of convergence to local minima, we use a continuation strategy. Specifically, the initial cost function yields the low-rank solution [8][1], while the continuation parameters are incremented to make the cost function approximate the desired one. We observe that this scheme is capable of overcoming local minima issues.

We demonstrate the utility of this scheme in free breathing perfusion MRI, free breathing cardiac MRI, and cardiac cine MRI (see figs. 1,2,3). Specifically, the use of relevant penalties on the dictionary provides improved basis functions, which translates to better reconstructions. Thus, this algo-

This work is supported by NSF CCF-0844812, NSF CCF-1116067, NIH 1R21HL109710-01A1 and ACS RSG-11-267-01-CCE.

[1] If $\mathcal{T}_1$ and $\mathcal{T}_2$ are energy preserving operators (eg. orthogonal transforms, tight frames).

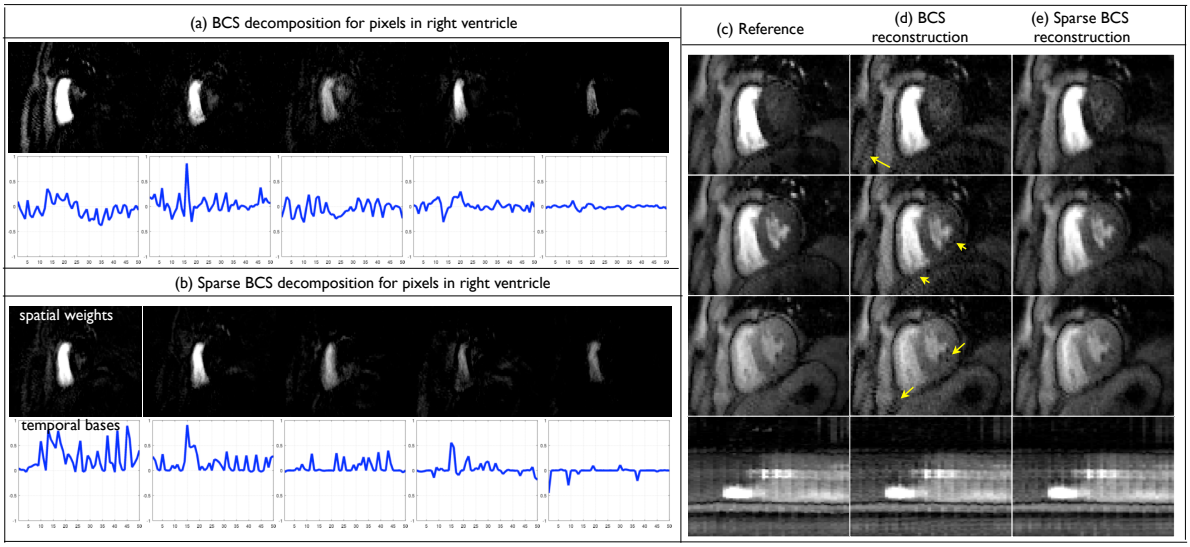

Fig. 1: Comparison of the sparse blind CS model with the blind CS model: An undersampling reconstruction experiment on a reference myocardial free breathing perfusion MRI data is performed. An example of the estimated spatial coefficients $u_i(\mathbf{x})$ and temporal basis functions $v_i(t)$ for the pixels belonging to the right ventricle are shown for the two models. Few image frames and the image time profiles are shown for the reference, BCS, sparse BCS models in (c,d,e). Temporal intensity variation patterns corresponding to contrast uptake (see the second basis function in both the models), and motion (see periodic ripples corresponding to breathing motion) are depicted well in both the models. However, few bases in BCS also contain random oscillations due to noise (ex: the fifth basis function in (a)). This leads to noise like artifacts in the resulting BCS reconstructions (see arrows in (d)). In contrast, the sparse BCS scheme penalizes the noise patterns, and the reconstructions are devoid of such artifacts while maintaining the temporal fidelity.

rithm can be customized to different applications by appropriately choosing the sparsity transforms or operators $(\mathcal{T}_1, \mathcal{T}_2)$. More importantly, we observe that choosing $\mathcal{T}_2$ as the temporal derivative operator yields comparable or even better reconstructions in the cardiac cine example, when compared with sparse recovery using the almost optimal Fourier dictionary (the k-t FOCUSS scheme).

2. BLIND CS WITH SPARSE DICTIONARIES

2.1. Dynamic image acquisition

The main goal is to recover the dynamic dataset $\gamma(\mathbf{x}, t) : \mathbb{Z}^3 \rightarrow \mathbb{C}$ from its under-sampled Fourier measurements. We represent the dataset as the $M \times N$ Casorati matrix [2]:

$$\mathbf{\Gamma}_{M\times N} = \begin{pmatrix} \gamma(\mathbf{x}_1, t_1) & . & . & . & \gamma(\mathbf{x}_1, t_N) \\ \gamma(\mathbf{x}_2, t_1) & . & . & . & \gamma(\mathbf{x}_2, t_N) \\ . & . & . & . & . \\ \gamma(\mathbf{x}_M, t_1) & . & . & . & \gamma(\mathbf{x}_M, t_N) \end{pmatrix}. \quad (1)$$

Here, M is the number of voxels in the image and N is the number of image frames in the dataset. The columns of $\mathbf{\Gamma}$ correspond to the voxels of each time frame. We model the measurement process as:

$$\mathbf{b}_i = \mathcal{A}_i(\mathbf{\Gamma}) + \mathbf{n}_i;\ i = 1, ..., N; \quad (2)$$

where, $\mathbf{b}_i$ and $\mathbf{n}_i$ are respectively the measurement and noise vectors at the i^{th} time instants. $\mathcal{A}_i$ is the Fourier sampling operator that evaluates the two dimensional Fourier transform of the i^{th} column of $\mathbf{\Gamma}$ on a specified sampling trajectory.

2.2. Image reconstruction

We model $\mathbf{\Gamma}$ as the product of a spatial coefficient matrix $\mathbf{U}_{M\times R}$ and a dictionary matrix $\mathbf{V}_{R\times N}$, which contains the temporal basis functions:

$$\mathbf{\Gamma}_{M\times N} = \mathbf{U}_{M\times R}\mathbf{V}_{R\times N}; \quad (3)$$

Here, R is the number of basis functions in the dictionary. We impose sparsity constraints on $\mathbf{U}$ and $\mathbf{V}$ in transform basis $\mathcal{T}_1, \mathcal{T}_2$ and simultaneously estimate them by solving:

$$\{\hat{\mathbf{U}}, \hat{\mathbf{V}}\} = \min_{\mathbf{U},\mathbf{V}} \|\mathcal{A}_i(\mathbf{UV}) - \mathbf{b}_i\|_2^2 + \lambda_1\|\mathcal{T}_1(\mathbf{U})\|_{\ell_1} + \lambda_2\|\mathcal{T}_2(\mathbf{V})\|_{\ell_1} \quad (4)$$

The first term ensures data consistency. The operators $\mathcal{T}_1, \mathcal{T}_2$ can be chosen appropriately based on the specific DMRI application. In this paper we considered the cases of (i)$\mathcal{T}_1 = \mathcal{I}, \mathcal{T}_2 = \mathcal{I}$, and (ii) $\mathcal{T}_1 = \mathcal{I}, \mathcal{T}_2 = \nabla_t$ (temporal derivative operator) respectively for regimes with large interframe motion (eg: free breathing MRI), and smooth temporal patterns (eg: cardiac cine). The main difference with the BCS setting is the sparsity constraint on $\mathbf{V}$ instead of the Frobenius norm constraint on $\mathbf{V}$. The motivation of imposing this additional sparsity constraint on the dictionary is demonstrated on a free breathing cardiac perfusion dataset in figure 1. The sparsity

constraint effectively penalizes the basis functions that capture noisy oscillations, which are present in the BCS setting. This translates to improved reconstructions where the noise like features (see arrows in Fig. 1 d) are reduced without compromising on the temporal fidelity.

2.3. Optimization algorithm

The problem in (4) contains the non-dfferentiable l_1 norms. To solve it, we first approximate the l_1 semi-norms by differentiable Huber induced penalties as:

$$\{\hat{\mathbf{U}},\hat{\mathbf{V}}\} = \min_{\mathbf{U},\mathbf{V}} ||\mathcal{A}_i(\mathbf{UV})-\mathbf{b}_i||_2^2+\lambda_1 \underbrace{\varphi_{\beta_1}(\mathcal{T}_1\mathbf{U})}_{\approx\|\mathcal{T}_1\mathbf{U}\|_1}+\lambda_2 \underbrace{\psi_{\beta_2}(\mathcal{T}_2\mathbf{V})}_{\approx\|\mathcal{T}_2\mathbf{V}\|_1}, \tag{5}$$

where, $\varphi_{\beta_1}(\mathcal{T}_1\mathbf{U}) = \sum_{i=1}^{M}\sum_{j=1}^{R} h_{\beta_1}(p_{i,j})$ and $\psi_{\beta_2}(\mathcal{T}_2\mathbf{V}) = \sum_{i=1}^{R}\sum_{j=1}^{N} h_{\beta_2}(q_{i,j})$ are the Huber-induced penalties; ($p_{i,j}, q_{i,j}$ are the entries of $\mathcal{T}_1\mathbf{U}$ and $\mathcal{T}_2\mathbf{V}$ respectively). The Huber function is specified as:

$$h_\beta(x) = \begin{cases} |x| - 1/2\beta & \text{if} \quad |x| \geq \frac{1}{\beta} \\ \beta\,|x|^2/2 & \text{else}\,. \end{cases} \tag{6}$$

When $\beta_1, \beta_2 \to \infty$, the Huber penalty approximates the l_1 semi norm, and hence the problem in (5) approximates the original problem in (4). However in practice, we observe that the algorithm is vulnerable to local minima if we solve for (5) with $\beta_1, \beta_2 \to \infty$. This is expected since (4) is not a convex optimization scheme. Hence, we use a continuation strategy to minimize the risk of local minima. We initially solve (5) for low values of β_1, β_2, during which (5) is a much simpler problem (quadratic in $\mathbf{U}$, $\mathbf{V}$), and progressively increase the complexity by incrementing β_1, β_2.

We rely on the majorize minimize framework to realize an efficient optimization algorithm. We start by majorizing the Huber induced penalties in (5):

$$\varphi_{\beta_1}(\mathcal{T}_1\mathbf{U}) = \min_{\mathbf{L}} \frac{\beta_1}{2}\|\mathcal{T}_1(\mathbf{U}) - \mathbf{L}\|_F^2 + \|\mathbf{L}\|_1, \tag{7}$$

$$\psi_{\beta_2}(\mathcal{T}_2\mathbf{V}) = \min_{\mathbf{R}} \frac{\beta_2}{2}\|\mathcal{T}_2(\mathbf{V}) - \mathbf{R}\|_F^2 + \|\mathbf{R}\|_1, \tag{8}$$

where $\mathbf{L}, \mathbf{R}$ are auxiliary variables. Substituting (7), (8) in (5), we obtain the following modified cost function, which has to be minimized with respect to four variables $\mathbf{U}$, $\mathbf{V}$, $\mathbf{L}$ and $\mathbf{R}$:

$$\min_{\mathbf{U},\mathbf{V},\mathbf{L},\mathbf{R}} \|\mathcal{A}_i(\mathbf{UV})-\mathbf{b}_i\|_2^2+\lambda_1\left(\frac{\beta_1}{2}\|\mathcal{T}_1(\mathbf{U}) - \mathbf{L}\|_F^2 + \|\mathbf{L}\|_1\right) + \lambda_2\left(\frac{\beta_2}{2}\|\mathcal{T}_2(\mathbf{V}) - \mathbf{R}\|_F^2 + \|\mathbf{R}\|_1\right); \tag{9}$$

While this formulation may appear more complex than the original problem in (4), this results in a simple algorithm. Specifically, we use an alternating minimization scheme to solve (9). At each step, we solve for a specific variable, assuming the other variables to be fixed; we systematically cycle through these subproblems until convergence.

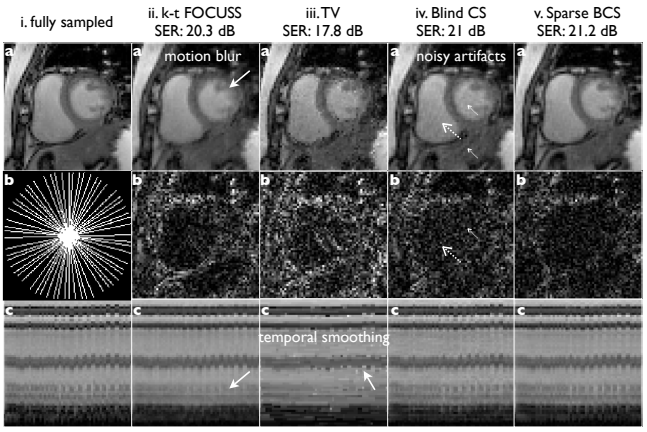

Fig. 2: Validation using realtime free breathing data: The rows (a), (b), (c) correspond to a specific spatial frame, the corresponding error image, and the temporal profile along a line. The sampling mask for one frame is shown in i.b. The error images are scaled up by ≈ 5 fold for better visualization. The k-t FOCUSS and TV constrained methods result in compromised reconstructions with reduced temporal fidelity due to the presence of large inter-frame breathing motion. The BCS scheme preserves the motion content. However the reconstructions suffer from noisy artifacts due to learning of noisy bases (see arrows in iv). In contrast, the sparse BCS scheme has reduced noise patterns while maintaining similar temporal fidelity compared to BCS.

The subproblems for $\mathbf{L}$ and $\mathbf{R}$ respectively involves shrinkage of $\mathcal{T}_1\mathbf{U}$ and $\mathcal{T}_2\mathbf{V}$. They can be solved analytically as:

$$\mathbf{L}_{n+1} = \frac{\mathcal{T}_1(\mathbf{U}_n)}{|\mathcal{T}_1(\mathbf{U}_n)|}\left(|\mathcal{T}_1(\mathbf{U}_n)| - \frac{1}{\beta_1}\right)_+; \tag{10}$$

$$\mathbf{R}_{n+1} = \frac{\mathcal{T}_2(\mathbf{V}_n)}{|\mathcal{T}_2(\mathbf{V}_n)|}\left(|\mathcal{T}_2(\mathbf{V}_n)| - \frac{1}{\beta_2}\right)_+; \tag{11}$$

where '+' represents the shrinkage operator defined as $(\tau)_+ = \max\{0, \tau\}$. The subproblems for $\mathbf{U}$ and $\mathbf{V}$ are quadratic. We solve them by using conjugate gradient (CG) algorithms. Starting with random matrix initializations of $\mathbf{U}$ and $\mathbf{V}$, the algorithm iterates between the $\mathbf{L}, \mathbf{R}, \mathbf{U}, \mathbf{V}$ subproblems in an inner loop, while progressively updating β_1, β_2 starting with small values in an outer loop. The inner loop is terminated when the cost in (4) stagnates. The outer loop is terminated when a large enough β_1, β_2 are achieved.

3. RESULTS

We evaluate the proposed scheme by performing retrospective undersampling experiments on fully sampled datasets.

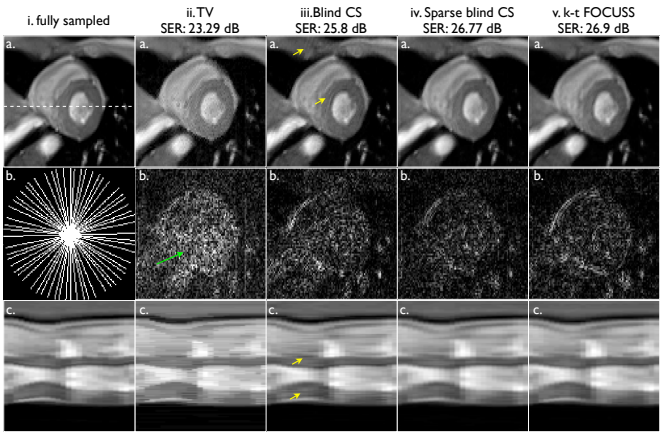

Fig. 3: Validation using cine data: The rows (a), (b), (c) correspond to a spatial frame during systole, the corresponding reconstruction error image, and the image time profile for different methods. The error images are scaled up by 9 fold for better visualization. The sampling trajectory for one frame is shown in (i).b. TV exhibits suboptimal reconstructions due to patchy artifacts along time. BCS shows subtle noise like oscillations (see the yellow arrows in (iii a,c) due to few noisy temporal basis functions. The sparse BCS scheme has reduced noisy artifacts and better temporal fidelity. We observe that the SER of sparse BCS is similar to k-t FOCUSS. However, note that the errors are diffused over the entire image in sparse BCS, while they are concentrated on the borders of the heart in k-t FOCUSS.

Specifically, we show one example with significant inter-frame motion content (free breathing MRI: $N_x \times N_y \times N_t = 128 \times 128 \times 60$: fig 2), and one with smooth temporal intensity variation (breath held cardiac cine MRI: $N_x \times N_y \times N_t = 156 \times 192 \times 25$: fig 3). A radial trajectory with 30 radial rays with golden ratio angle spacing between successive rays was used for undersampling. We perform comparisons with k-t FOCUSS [4], temporal total variation (TV) constrained reconstruction [5], and blind CS [7]. We considered 30 basis functions in the blind CS and the sparse blind CS models. The sparse blind CS model was implemented with $\mathcal{T}_1 = \mathcal{I}, \mathcal{T}_2 = \mathcal{I}$ in Fig. 2, and with $\mathcal{T}_1 = \mathcal{I}, \mathcal{T}_2 = \nabla_t$ in Fig. 3. The values of the regularization parameters in all the methods were chosen such that the signal to error ratio between the reconstruction and the reference fully sampled data was maximized ($SER : 10\log_{10} \|\mathbf{\Gamma}_{\text{ideal}}\|_2^2 / \|\mathbf{\Gamma}_{\text{ideal}} - \mathbf{\Gamma}_{\text{recon}}\|_2^2$).

In Fig. 2, we observe the kt FOCUSS and the TV methods are suboptimal due to the large motion content. Specifically, they exhibit poor temporal fidelity due to motion blur and temporal smoothing. The BCS scheme is robust to these compromises and preserves the motion well. However, due to few of the bases learning the noise patterns, the BCS reconstructions suffer from noise like pixelated artifacts (see arrows in Fig. 2iv). In contrast the sparse BCS scheme penalizes these noisy patterns, thus providing superior reconstructions.

The experiment on cine data in Fig. 3 was done at a high acceleration of ≈ 6.4. We observe TV to be suboptimal at this acceleration. This behavior was also observed in the studies in [9]. It had patchy artifacts along time which highlight as speckles in the reconstructions. We observe the BCS scheme to exhibit subtle noisy pixelations as some of the bases captured noise. However, when we constrain the learned basis functions to be smooth, the reconstructions improve considerably. The sparse BCS model had similar SER when compared to kt FOCUSS but the pattern of error distributions are very different. The former had more diffused errors, while kt FOCUSS had errors concentrated on the borders of the heart.

4. CONCLUSION

We proposed a new algorithm to learn dictionary elements that are sparse in pre-specified transform domains from under sampled k-space data for dynamic MRI reconstruction. A majorize minimize algorithm with continuation was developed to solve the resulting optimization problem efficiently. Our results suggest that noise patterns in the learned basis functions can be considerably reduced by promoting sparsity of the dictionary in an appropriate transform basis. Through various examples, we demonstrated the better performance of the proposed method over current dynamic imaging schemes.

5. REFERENCES

[1] B. Madore, "Using unfold to remove artifacts in parallel imaging and in partial-fourier imaging," *Magn Reson Med*, vol. 48, no. 3, pp. 493–501, Sep 2002.

[2] Z. Liang, "Spatiotemporal imagingwith partially separable functions," in *Biomedical Imaging: From Nano to Macro, 2007. ISBI 2007. 4th IEEE International Symposium on*. IEEE, 2007, pp. 988–991.

[3] S. Lingala, Y. Hu, E. DiBella, and M. Jacob, "Accelerated dynamic mri exploiting sparsity and low-rank structure: k-t slr," *IEEE Transactions on Medical Imaging*, vol. 30, no. 5, pp. 1042–1054, 2011.

[4] H. Jung, J. Park, J. Yoo, and J. C. Ye, "Radial k-t focuss for high-resolution cardiac cine mri," *Magn Reson Med*, Oct 2009.

[5] G. Adluru, S. Awate, T. Tasdizen, R. Whitaker, and E. DiBella, "Temporally constrained reconstruction of dynamic cardiac perfusion mri," *Magnetic Resonance in Medicine*, vol. 57, no. 6, pp. 1027–1036, 2007.

[6] B. Zhao, J. Haldar, A. Christodoulou, and Z. Liang, "Image reconstruction from highly undersampled (k, t)-space data with joint partial separability and sparsity constraints." *IEEE transactions on medical imaging*, 2012.

[7] S. Lingala and M. Jacob, "A blind compressive sensing frame work for accelerated dynamic mri," in *Biomedical Imaging (ISBI), 2012 9th IEEE International Symposium on*. IEEE, 2012, pp. 1060–1063.

[8] B. Recht, M. Fazel, and P. Parrilo, "Guaranteed minimum-rank solutions of linear matrix equations via nuclear norm minimization," *Arxiv preprint arxiv:0706.4138*, 2007.

[9] C. Bilen, Y. Wang, and I. Selesnick, "Compressed sensing for moving imagery in medical imaging," *arXiv preprint arXiv:1203.5772*, 2012.